Materials Research Proceedings 57 (2025) 344-351 https://doi.org/10.21741/9781644903735-40

Peripheral coarse grain prediction in extruded AA6082: Combining finite element simulations with neural networks

Marco Negozio[1,a *], Adrian H.A. Lutey[1,b], Antonio Segatori[2,c], Riccardo Pelaccia[3,d], Sara Di Donato[4,e], Barbara Reggiani[3,5f] and Lorenzo Donati[4,g]

[1]University of Parma - DISTI Department for Industrial Systems and Technologies, Parco Area delle Scienze, 181/A, 43124 Parma, Italy

[2]Hydro, Innovation and Technology, Myrkärrsvägen 1, 612 31 Finspång, Sweden

[3]University of Modena and Reggio Emilia - DISMI Department of Sciences and Methods for Engineering, Via Amendola 2, 42122, Reggio Emilia, Italy

[4]University of Bologna - DIN Department of Industrial Engineering, Viale Risorgimento 2, 40136, Bologna, Italy

[5]University of Modena and Reggio Emilia - InterMech - MO.RE, Piazzale Europa 1, Reggio Emilia 42124, Italy

[a]marco.negozio@unipr.it, [b]adrian.lutey@unipr.it, [c]antonio.segatori@hydro.com, [d]riccardo.pelaccia@unimore.it, [e]sara.didonato2@unibo.it, [f]barbara.reggiani@unimore.it, [g]l.donati@unibo.it

Keywords: Aluminum Alloy Extrusion, Finite Element Simulation, Artificial Neural Network, Peripheral Coarse Grain, Microstructure Prediction

Abstract. Peripheral Coarse Grain (PCG) is a critical defect that affects the mechanical and crash performance of extruded AA6XXX aluminum profiles, particularly in automotive applications. Traditional methods to address this issue rely on extensive experimental campaigns, which are resource-intensive and often lead to conservative process parameters, reducing production efficiency. This study develops and validates a predictive model for PCG formation, combining finite element method (FEM) simulations and machine learning (ML) techniques. Data from FEM simulations and experiments were used to train and test a model employing artificial neural networks (ANNs) for PCG prediction. The proposed approach enables accurate PCG forecasting, providing a robust tool for optimizing process parameters, reducing reliance on empirical methods and advancing smart manufacturing solutions.

Introduction

The extrusion of AA6XXX aluminum alloys plays a crucial role in manufacturing lightweight structural components, particularly for the automotive industry, where mechanical strength and crash resistance are critical factors influencing structural integrity [1,2]. However, one of the most persistent challenges in this process is the formation of Peripheral Coarse Grain (PCG), which can significantly degrade mechanical properties and energy absorption performance [3–5]. The mechanisms behind PCG formation are complex, as they depend on a combination of process parameters, such as billet temperature, extrusion speed and die geometry, as well as metallurgical factors like chemical composition of the billet material, dispersoid distribution and recrystallization kinetics [6].

Previous studies have explored various strategies to mitigate PCG, primarily relying on experimental investigations that require significant time and resources [7]. Computational approaches, particularly those based on Finite Element Method (FEM) simulations, have been employed to analyze the thermomechanical conditions leading to PCG formation [8,9]. However, despite their potential, these models often struggle to provide accurate predictions across different

Materials Research Proceedings 57 (2025) 344-351 https://doi.org/10.21741/9781644903735-40

extrusion conditions. Recent advancements in machine learning (ML) have demonstrated promising results in improving the accuracy of predictions in the field of materials processing, particularly through the use of artificial neural networks (ANNs) that can be applied to large datasets, identifying complex relationships between variables [10,11].

In this work, three different extruded profiles in AA6082 alloy were analyzed experimentally, with microstructural observations carried out to measure PCG thickness in various positions within each profile. Data obtained from these experiments were then employed to train an ANN based on input data obtained via FEM simulations performed with commercial software package QForm Extrusion UK to predict the occurrence of PCG during the extrusion process.

The study aims to develop a framework for robust predictive modeling of PCG formation by integrating FEM simulations and ML techniques. The approach involves training ANNs using both numerical and experimental data to enhance predictive accuracy under diverse process conditions. By merging physics-based modeling and data-driven methodologies, this study provides an advanced tool for optimizing extrusion parameters, reducing dependency on iterative experimental methodologies and contributing to the development of intelligent manufacturing processes. The implementation of this predictive framework is expected to help industries improve the quality and efficiency of extruded aluminum components while minimizing risks associated with PCG formation.

Experimental Analysis

To validate the ANN developed for predicting microstructural evolution during extrusion, a hollow profile was produced using AA6082 alloy (Figure 1c). The extrusion process was conducted under five different sets of process parameters, with billet preheating temperatures of 450°C and 500°C. At 450°C, the ram speed was set to 5 mm/s and 15 mm/s, while at 500°C, tests were performed at 5 mm/s, 10 mm/s and 15 mm/s. The alloy chemical composition, homogenization parameters and press parameters including billet/tool dimensions and temperature distribution are reported in Table 1. Extrusion experiments were conducted in a strictly monitored environment to ensure correct acquisition of the extrusion load and profile exit temperature for validation of the FEM simulation. For ANN training, experimental data from two previously extruded profiles in the same alloy [8] were used (Figure 1a and 1b). The profile reported in this study served as an independent dataset to validate ANN prediction of the peripheral coarse grain defect.

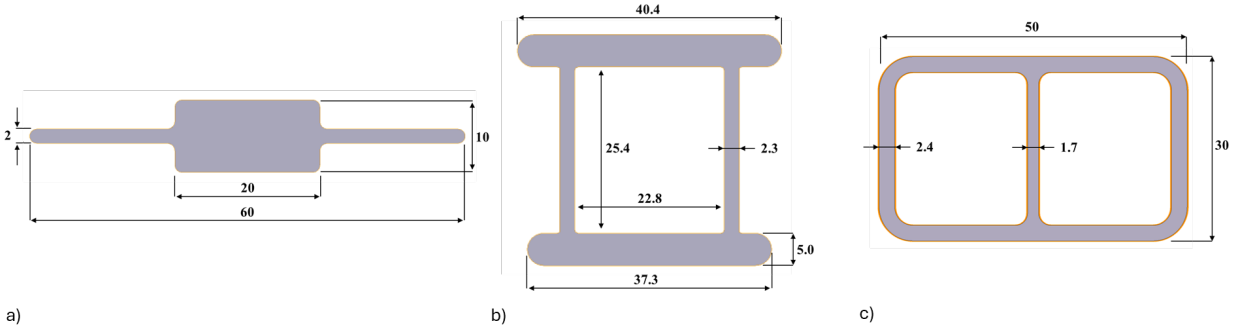

Figure 1: Geometry of a) Profile a; b) Profile b; c) Profile c.

Materials Research Proceedings 57 (2025) 344-351 https://doi.org/10.21741/9781644903735-40

Table 1: Process parameters employed for experiments.

Process parameters	Profile *a*	Profile *b*	Profile *c*
Press capacity [MN]	10	10	10
Aluminum alloy	AA6082	AA6082	AA6082
Extrusion ratio	18.2	31.5	21.9
Container temperature [°C]	410	410	410
Billet temperature [°C]	350 / 450 / 500	500	450 / 500
Die temperature [°C]	480	480	480
Billet length [mm]	400	350	400
Billet diameter [mm]	100	100	100
Billet Rest length [mm]	15	15	15
Billet Homogenization	565°C - 2h	565°C - 2h	565°C - 2h
Container diameter [mm]	107	107	107
Ram speed [mm/s]	2 / 5 / 10	2 / 5 / 10 / 15 / 20	5 / 10 / 15
Ram acceleration time [s]	5	5	5

Microstructural characterization was performed in the middle section of each extruded profile, where steady-state conditions were expected to be achieved in terms of temperature and velocity. Electrolytic etching (40 V dc, 4 min, 15 mL HBF_4 reagent, 750 mL H_2O), followed by image acquisition using the optical microscope Zeiss Axio Observer 3 was carried out to collect PCG data. The resulting micrographs were analyzed using ImageJ software to measure grain size and distribution. This analysis allowed direct comparison between predicted and experimentally observed microstructural features, providing insight into the model's accuracy and reliability.

Numerical Simulation

The extrusion process was simulated using QForm Extrusion UK. Within the software, a viscoplastic material model was employed to govern the process, meaning that material behavior was defined directly by a constitutive equation linking flow stress to strain, strain rate and temperature. Each individual extrusion experiment employing unique process parameters was investigated through a dedicated simulation. The Qshape tool within QForm was used to automatically generate and optimize the mesh for the tool components. Although standard mesh settings are generally recommended to balance precision and computational cost, simulations were performed with the finest available refinement to capture detailed process phenomena.

Material properties for AA6082 aluminum alloy employed in simulations are provided in [1]. The Hensel-Spittel law was employed to describe the flow behavior of AA6082. In this model, the flow stress, $\bar{\sigma}$, is expressed as a function of strain, $\bar{\varepsilon}$, strain rate, $\dot{\bar{\varepsilon}}$, and temperature T:

$$\bar{\sigma} = A \cdot e^{m_1 T} \cdot \bar{\varepsilon}^{-m_2} \cdot \dot{\bar{\varepsilon}}^{-m_3} \cdot e^{\frac{m_4}{\bar{\varepsilon}}} \cdot (1+\bar{\varepsilon})^{m_5 T} \cdot e^{m_7 \bar{\varepsilon}} \cdot \dot{\bar{\varepsilon}}^{m_8 T} \cdot T^{m_9} \quad (1)$$

For AA6082, parameter A is 280 MPa, while m_1 and m_5, which account for temperature effects, are –0.00461 K^{-1} and 0.00036 K^{-1}, respectively. Constants m_2, m_3, and m_4 are –0.16636, 0.12 and –0.02056, whereas m_7, m_8 and m_9 are all equal to zero [8].

Friction between the workpiece and tools was set based on optimized default values within Qform. Specifically, sticking conditions were applied at the billet interfaces with the container, ram and die, while the bearings were modeled using the Levanov friction model with m = 0.3 and n = 1.25.

Materials Research Proceedings 57 (2025) 344-351 https://doi.org/10.21741/9781644903735-40

Finally, to validate the simulation results, the predicted extrusion load and exit temperature of the profile were compared with experimental measurements. The exit temperature was recorded using a pyrometer aimed at the top-center of the investigated profiles. Discrepancies in both load and temperature predictions remained below 5%, underscoring the reliability of the simulation.

In accordance with the Negozio-Donati framework [12,13], parameters obtained directly from the FEM simulation were utilized to determine the maximum strain rate, $\dot{\varepsilon}_{max}$, Zener-Hollomon parameter, Z, subgrain size, δ, internal dislocation density, ρ_i, misorientation angle, Θ, stored energy, Pd, and percentage dynamic recrystallization, X_{DRX}. The approach for calculating the maximum strain rate was based on the procedure detailed in [13], which involves examining strain rate values at each time step throughout the deformation sequence from the initial billet to the final profile and determining the peak value. All remaining parameters were subsequently derived following the methodology described in [13], as outlined below.

$$\frac{1}{\delta} = C\,(lnZ)^n \tag{2}$$

$$Z = \dot{\varepsilon}_{max}\, exp\left(\frac{Q}{RT}\right) \tag{3}$$

$$\rho_i = \left(C_1 * Z^{C_2}\right) * (1 - e^{C_3 * \varepsilon}) \tag{4}$$

$$\Theta = (C_4 * Z^{C_5}) * (1 - e^{C_6 * \varepsilon}) \tag{5}$$

$$\mathrm{Pd} = \frac{Gb^2}{10}\left[\rho_i(1\text{-}\ln(10b\rho_i^{0,5})) + \frac{2\theta}{b\delta} * \left(1 + \ln\left(\frac{\theta c}{\theta}\right)\right)\right] \tag{6}$$

$$X_{DRX} = 1 - \exp\left[-\beta\left(\frac{\varepsilon - \varepsilon_c}{\varepsilon_s}\right)^m\right] \tag{7}$$

where T is the exit temperature, $C = 3.36\times10^{-9}$ m^{-1} and $n = 5.577$ are constants, Q is the activation energy of AA6082 (182000 J/mol·K), R is the universal gas constant (8.341 J/mol), G is the material shear modulus (2.05×10^{10} Pa), b is the Burgers vector (2.86×10^{-10} m) and Θc the misorientation angle limit (15°). For evaluation of the internal dislocation density, ρ_i, and misorientation angle, Θ, six material constants were determined from experimental data via regression (C_1= 328157965, C_2= 0.27, C_3= -5, C_4= 0.85, C_5= 0.05, C_6= -2.5). Finally, for calculation of X_{DRX}, ε_c is critical strain for DRX, ε_s is the saturated strain and β = 1.823 and m = 1.109 are material constants.

Figure 2 displays an example of FEM outcomes for extrusion of the Profile *c* with a billet temperature of 500 °C and ram speed of 15 mm/s. These results exhibit a generally symmetrical distribution for all investigated parameters across the two adjacent cavities. In particular, contour plots indicate that higher values tend to concentrate near the inner edges of cavities and along boundary regions, suggesting localized intensification of both stress and material flow. The temperature field appears relatively uniform, while plastic strain concentrates along the inner edges and corners where geometric discontinuities typically intensify stress. Stress-related fields exhibit pronounced peaks at corners, indicative of stress concentration that is typical in geometries with sharp transitions. The velocity exhibits a fairly balanced exit speed (velocity deviation < 5%) with negligible accelerated flow near the mid-plane between the cavities, gradually decreasing toward the outer edge. The percentage dynamic recrystallization (X_{DRX}) follows a similar pattern to plastic

Materials Research Proceedings 57 (2025) 344-351 https://doi.org/10.21741/9781644903735-40

strain, with relatively uniform regions in the bulk of the material and more pronounced gradients in proximity to the internal and external boundaries.

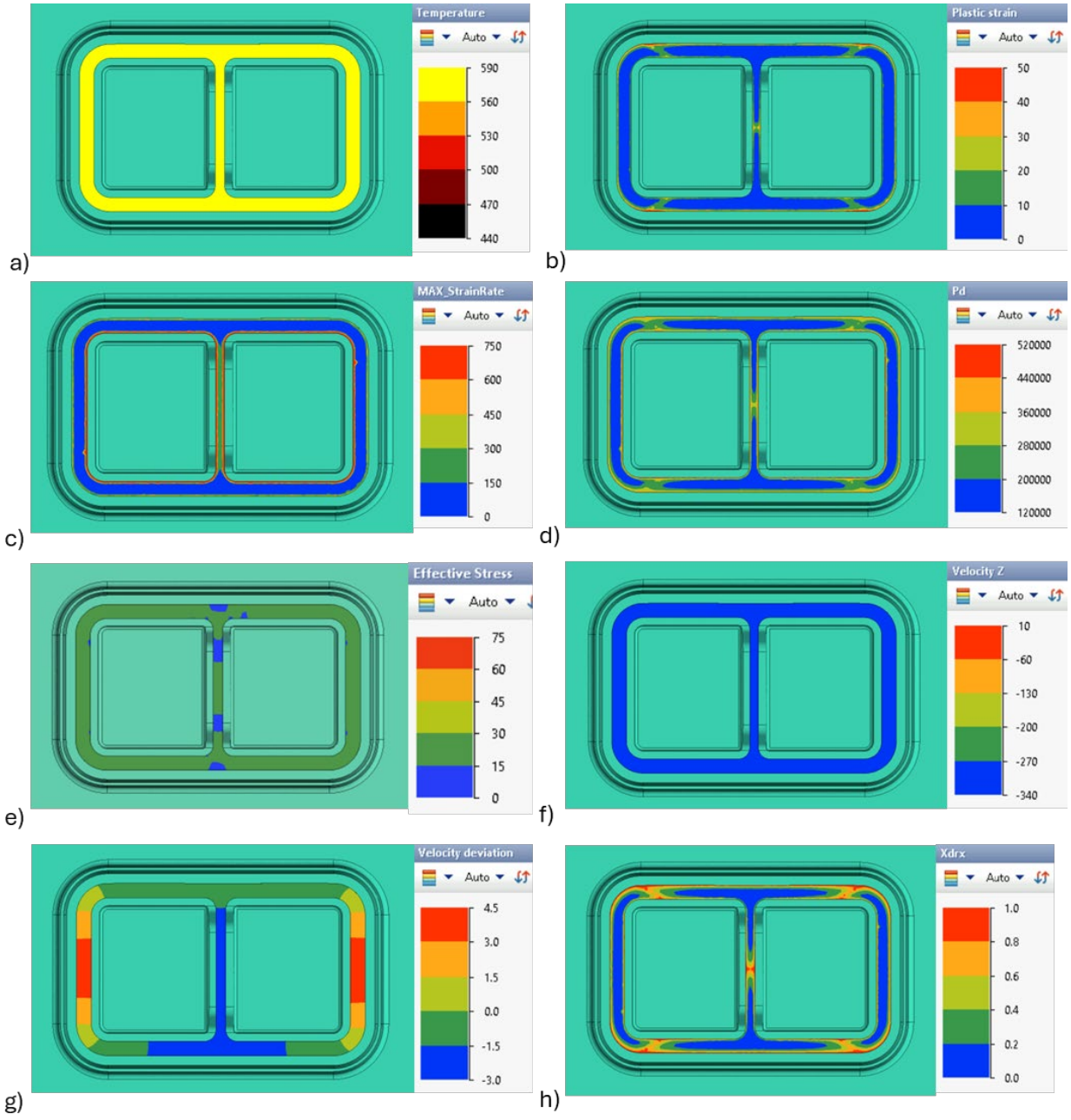

Figure 2: FEM outcomes for Profile c with a billet temperature of 500°C and ram speed of 15 mm/s: a) profile exit temperature, b) plastic strain, c) maximum strain rate, d) stored energy, e) effective stress, f) profile exit velocity, g) velocity deviation and h) $\boldsymbol{X_{DRX}}$.

ANN prediction model for PCG formation

A fully connected artificial neural network (ANN) for classification was trained for predicting PCG formation using simulation and experiment data from extrusion of Profiles *a* and *b* (Figure 1) in a previous study [8]. Training was performed with the *fitcnet* function in MATLAB employing the Broyden-Fletcher-Goldfarb-Shanno quasi-Newton algorithm (LBFGS) to minimize cross-entropy loss. Input parameters were considered as the exit temperature, strain, maximum strain rate, stored energy, percentage dynamic recrystallization, effective stress, velocity and

Materials Research Proceedings 57 (2025) 344-351 https://doi.org/10.21741/9781644903735-40

velocity deviation. The output parameter was considered as classification of PCG formation ('yes') or not ('no'). For training, labelled PCG data for Profiles *a* and *b* were employed as output data. Outcomes of hyperparameter optimization indicated that lowest cross-entropy loss was achieved with a single hidden layer with 22 neurons and a ReLU activation function. This configuration was employed for the final ANN employed to predict PCG formation in Profile *c*.

Results and Discussion

Figure 3 presents the microstructures of Profile *c* extruded with different process parameters. The outcomes are consistent with those reported in [8]. In particular, PCG formation is localized in regions where both the strain and maximum strain rate are highest, exhibiting notable correlation with the strain rate. For instance, when comparing microstructures obtained at the same extrusion speed but at different temperatures (e.g., Figure 3a and 3c, or Figure 3b and 3e), similar PCG thicknesses are observed. Moreover, analysis of Figure 3d and 3e reveals that increasing the ram speed from 10 mm/s to 15 mm/s does not significantly alter the PCG thickness, whereas a change is evident when increasing the speed from 5 mm/s to 10 mm/s (see Figure 3c and 3d). These results align with previous findings by the authors [6–8,14], where a proportional relationship between the ram speed and PCG thickness was identified up to a critical ram velocity. Beyond this threshold, the thickness remains essentially constant, likely due to the fact that the ram speed is not the sole factor governing PCG formation; temperature, plastic strain and consequently X_{DRX} must also exceed certain threshold levels.

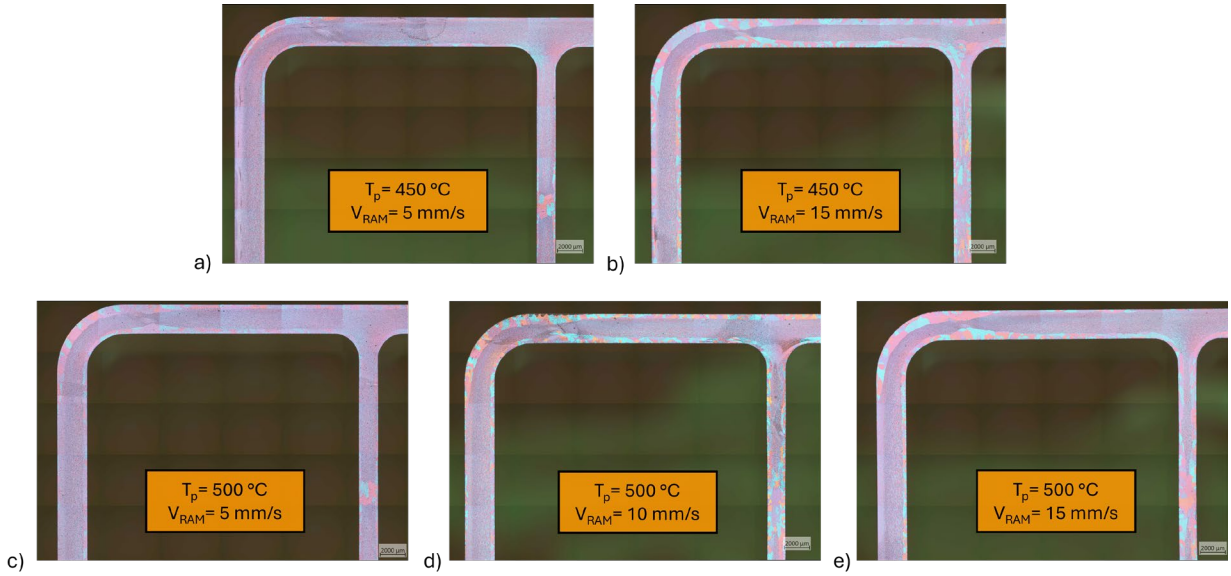

Figure 3: Cross-section images of extruded Profile c under different process conditions: a) T = 450 °C, V_{ram} = 5 mm/s; b) T = 450 °C, V_{ram} = 15 mm/s; c) T = 500 °C, V_{ram} = 5 mm/s; d) T = 500 °C, V_{ram} = 10 mm/s; e) T = 500 °C, V_{ram} = 15 mm/s.

Figure 4 presents maps of ANN predictions of PCG formation under the same conditions as in Figure 3. Marked alignment between predicted and experimental outcomes is evident both in terms of PCG extension and location. Figure 4a and 4b present extruded profiles obtained at a billet temperature of 450 °C, whereas Figure 4c, 4d and 4e correspond to a billet temperature of 500 °C. ANN predictions effectively capture the overall trend of experimental PCG formation, which increases proportionally to extrusion speed. However, some discrepancies can be observed at 15 mm/s, where predicted PCG formation at 450 °C is more extensive than in micrographs, despite similarities in PCG zones in both cases. Nonetheless, these differences do not compromise the overall accuracy of the prediction, especially considering that the analyzed scenario represents a

Materials Research Proceedings 57 (2025) 344-351 https://doi.org/10.21741/9781644903735-40

test case, thereby underscoring the value of the combined FEM and ANN approach. Further developments are warranted to generate a balanced training dataset comprising extruded profiles with varying dimensions produced under different process parameters. The implications of these outcomes in an industrial production setting are significant, with ANN prediction of PCG formation paving the way for rapid process optimization with next-generation digital tools.

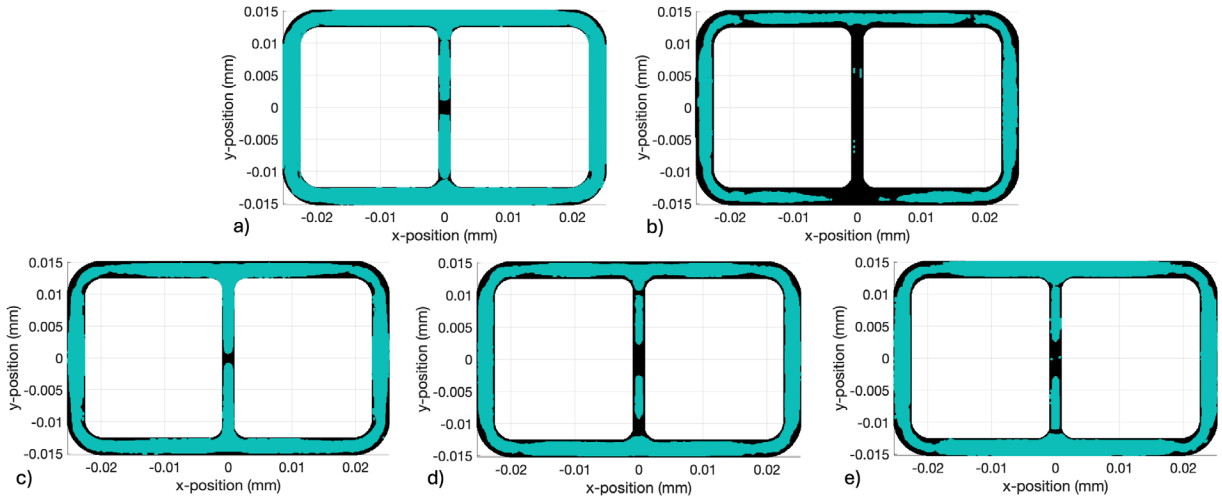

Figure 4: PCG prediction maps of extruded Profile c under different processing conditions: a) T = 450 °C, V_{ram} = 5 mm/s; b) T = 450 °C, V_{ram} = 15 mm/s; c) T = 500 °C, V_{ram} = 5 mm/s; d) T = 500 °C, V_{ram} = 10 mm/s; e) T = 500 °C, V_{ram} = 15 mm/s. PCG formation shown in black.

Conclusion

The present study has demonstrated integration of FEM simulations with ANNs to predict PCG formation in extruded profiles. The developed ANN was trained on both simulation and experimental data from two different AA6082 extruded profiles (Profiles *a* and *b*), utilizing eight input parameters including exit temperature, strain, maximum strain rate, stored energy, percentage dynamic recrystallization, effective stress, velocity and velocity deviation to classify PCG formation.

Experimental analysis of Profile *c*, extruded at billet temperatures of 450 °C and 500 °C and ram speeds of 5, 10 and 15 mm/s, confirmed that PCG formation was localized in regions of high strain and strain rate. Quantitatively, a proportional increase in PCG thickness with ram speed was observed up to a critical threshold, beyond which additional speed increases (e.g., from 10 mm/s to 15 mm/s) produced minimal changes in thickness. While the overall trends of predictions obtained with the trained ANN closely matched experimental observations, a slight discrepancy was noted at a billet temperature of 450 °C and ram speed of 15 mm/s, where the model indicated a higher extent of PCG formation compared to that observed in micrographs. Despite this minor deviation, the ANN prediction remained robust, particularly considering that the analyzed scenario served as a test case. These outcomes validate the effectiveness of the combined FEM and ANN approach for predicting microstructural phenomena, highlighting its potential for rapid process optimization. Future work will focus on generating a balanced training dataset, including extruded profiles of varying dimensions and processing parameters, to further enhance model accuracy and industrial applicability.

References

[1] Negozio M, Pelaccia R, Donati L, Reggiani B. Numerical investigation of the surface recrystallization during the extrusion of a AA6082 aluminum alloy under different process

conditions. Int J Adv Manuf Technol 2023;129:1585–99. https://doi.org/10.1007/s00170-023-12397-8

[2] Donati L, Reggiani B, Pelaccia R, Negozio M, Di Donato S. Advancements in extrusion and drawing: a review of the contributes by the ESAFORM community. Int J Mater Form 2022;15:41. https://doi.org/10.1007/s12289-022-01664-w

[3] Li Z, Qin J, Zhang H, Wang X, Zhang B, Nagaumi H. Improved Distribution and Uniformity of α-Al(Mn,Cr)Si Dispersoids in Al-Mg-Si-Cu-Mn (6xxx) Alloys by Two-Step Homogenization. Metall Mater Trans A 2021;52:3204–20. https://doi.org/10.1007/s11661-021-06243-3

[4] Qian X, Parson N, Chen X-G. Effects of Mn addition and related Mn-containing dispersoids on the hot deformation behavior of 6082 aluminum alloys. Mater Sci Eng A 2019;764:138253. https://doi.org/10.1016/j.msea.2019.138253

[5] Negozio M. Experimental analysis and modeling of the recrystallization behaviour of a AA6060 extruded profile, 2023, p. 477–86. https://doi.org/10.21741/9781644902479-52

[6] Eivani AR, Zhou J. Application of physical and numerical simulations for interpretation of peripheral coarse grain structure during hot extrusion of AA7020 aluminum alloy. J Alloys Compd 2017;725:41–53. https://doi.org/10.1016/j.jallcom.2017.06.297

[7] Eivani AR, Zhou J, Duszczyk J. Mechanism of the formation of peripheral coarse grain structure in hot extrusion of Al-4.5Zn-1Mg. Philos Mag 2016;96:1188–96. https://doi.org/10.1080/14786435.2016.1157637

[8] Negozio M, Segatori A, Pelaccia R, Reggiani B, Donati L. Experimental investigation and numerical prediction of the peripheral coarse grain (PCG) evolution during the extrusion of different AA6082 aluminum alloy profiles. Mater Charact 2024;209:113723. https://doi.org/10.1016/j.matchar.2024.113723

[9] Eivani AR, Jafarian HR, Zhou J. Simulation of peripheral coarse grain structure during hot extrusion of AA7020 aluminum alloy. J Manuf Process 2020;57:881–92. https://doi.org/10.1016/j.jmapro.2020.07.011

[10] Negozio M, Ferraro V, Donati L, Lutey AHA. Predicting grain size in extruded AA6063 profiles: A unified approach based on finite element analysis and machine learning. Int J Adv Manuf Technol 2024;133:4543–60. https://doi.org/10.1007/s00170-024-14021-9

[11] Shang H, Wu P, Lou Y, Wang J, Chen Q. Machine learning-based modeling of the coupling effect of strain rate and temperature on strain hardening for 5182-O aluminum alloy. J Mater Process Technol 2022;302:117501. https://doi.org/10.1016/j.jmatprotec.2022.117501

[12] Negozio M, Pelaccia R, Donati L, Reggiani B. Simulation of the microstructure evolution during the extrusion of two industrial-scale AA6063 profiles. J Manuf Process 2023;99:501–12. https://doi.org/10.1016/j.jmapro.2023.05.075

[13] Negozio M, Segatori A, Pelaccia R, Reggiani B, Donato SD, Donati L. Modeling of recrystallization behaviour of AA6xxx aluminum alloy during extrusion process. Trans Nonferrous Met Soc China 2024;34:3170–84. https://doi.org/10.1016/S1003-6326(24)66600-8

[14] Negozio M, Di Donato S, Pelaccia R, Lutey AH, Carosi D, Reggiani B, et al. Impact of die design and bearing geometry on grain size and PCG formation during extrusion of AA6082 aluminum alloy. J Mater Sci Technol 2025;230:80–92. https://doi.org/10.1016/j.jmst.2025.01.017